SAND2018-13343J

Electrolyte-Assisted Hydrogen Storage Reactions

John J. Vajo[1], Hongjin Tan[2**], Channing C. Ahn[2,3], Dan Addison[2], Son-Jong Hwang[4],*

James L. White[5], Timothy C. Wang[5], Vitalie Stavila[5], Jason Graetz[1]

1) HRL Laboratories, LLC, 3011 Malibu Canyon Road, Malibu, CA 90265

2) Liox Power, Inc., 129 North Hill Ave., Suite 107, Pasadena, CA 91106

3) Division of Engineering and Applied Science, California Institute of Technology, Pasadena, CA 91125

4) Division of Chemistry and Chemical Engineering, California Institute of Technology, Pasadena, CA 91125

5) Sandia National Laboratories, P.O. Box 969, Livermore, CA, 94551

Corresponding Author

* jjvajo@hrl.com

Abstract

Use of electrolytes, in the form of Li/KBH_4 and Li/K/CsI eutectics, is shown to significantly improve (by more than a factor of ten) both the dehydrogenation and full rehydrogenation of the MgH_2/Sn destabilized hydride system and the hydrogenation of MgB_2 to $Mg(BH_4)_2$. The improvement revealed that inter-particle transport of atoms heavier than hydrogen can be an important rate-limiting step during hydrogen cycling in hydrogen storage materials consisting of multiple phases in powder form. Electrolytes enable solubilizing heavy ions into a liquid environment and thereby facilitate the reaction over full surface areas of interacting particles. The examples presented suggest that use of electrolytes in the form of eutectics, ionic liquids, or solvents containing dissolved salts may be generally applicable for increasing reaction rates in complex and destabilized hydride materials.

Introduction

Hydrogen cycling in high capacity hydrogen storage materials often involves multiple solid phases in powder-particle form that must interact, nucleate, grow, and shrink during reaction. These materials, including many complex hydrides[1-3] and destabilized hydride mixtures[4] (also called reactive hydride composites[5]), have rates of hydrogen uptake and release that are typically very slow. To address this issue, catalytic additives[6] and nanoscale formulations[7-9] have been studied extensively. These approaches have produced considerable improvements, although the rates of hydrogen cycling are still typically too limited for practical applications, such as vehicular hydrogen storage. One reason for this limitation may be that both catalytic additives and nanoscale formulations predominately address atomic transport and reaction within individual particles. However, in multiple solid-phase materials, atomic transport between particles of different phases is required. This requirement could impose additional kinetic restrictions because inter-particle transport 1) likely involves the motion of atoms heavier than hydrogen, such as Li, Na, Mg, B, and Al; 2) may occur over relatively long distances (much longer than typical bond lengths); and 3) can only occur at interfaces where different phase particles come in contact on an atomic scale. For typical powders, this interfacial area may be only a small fraction of the total surface area.

Here we explore the idea that the kinetics of hydrogen cycling in multiple-phase hydrogen storage materials may be improved through the addition of a liquid electrolyte. The electrolyte may assist inter-particle transport and promote the overall reaction (addressing the restrictions listed above) by 1) solubilizing reacting ions; 2) providing liquid-state diffusion rates facilitating long distance transport; and 3) giving transported ions access to the full surface area of the reacting phases by surface wetting, effectively greatly increasing the area over which reaction can occur.

We show that using electrolytes can significantly increase the rates of dehydrogenation and hydrogenation, by factors of ~10× or more. This increase clearly identifies the role of inter-particle transport in governing the overall rates and mechanisms of hydrogen exchange and may provide a useful step towards the eventual commercial application of these materials by enabling cycling under more moderate conditions closer to equilibrium.

Although to our knowledge, this idea has not been explored explicitly, this work builds upon prior studies that have considered systems in which hydrides were dissolved in solvents[10-14], solvate-type hydride adducts were formed[15-20], and molten phases were reported to participate in reaction[21-23].

Results

To illustrate the influence of an electrolyte on hydrogen cycling in multiple phase hydrogen storage materials we describe results for two systems: MgH_2/Sn and $Mg(BH_4)_2$. The MgH_2/Sn system is a prototypical destabilized hydride in which Sn lowers the enthalpy for dehydrogenation through the formation of Mg_2Sn. During dehydrogenation, MgH_2 and Sn, typically milled together as powders, interact to release hydrogen and form Mg_2Sn. Upon rehydrogenation, hydrogen interacts with Mg_2Sn to reform separate phases of MgH_2 and Sn. This reaction[24-26], and to a greater extent its analog, MgH_2/Si[24-29], have been studied and found to dehydrogenate with the formation of Mg_2Sn (and Mg_2Si), although only at temperatures well above predicted equilibrium temperatures. Rehydrogenation has not been observed to any significant extent in previous studies. $Mg(BH_4)_2$ is a complex hydride that is potentially practical due to its high theoretical hydrogen content of 14.9 wt% H_2 and favorable equilibrium pressure of 1 bar at ~100 °C.[30,31] Although initially single phase, its dehydrogenation pathway is complex, with the formation of multiple intermediate phases

such as $MgB_{12}H_{12}$ and MgH_2. These phases must further interact, ultimately forming MgB_2.[30] Significant (>70%) hydrogenation of MgB_2 has been achieved although only under impractical conditions, e.g., ~1000 bar H_2 at ~400 °C.[32] Therefore, it is highly desirable to facilitate the rehydrogenation of this system at some more achievable set of conditions.

Electrolyte-assisted hydrogen cycling in MgH_2/Sn. Dehydrogenation of milled mixtures of MgH_2 + 0.5Sn (theoretical capacity 2.3 wt% H_2) with and without an electrolyte composed of the eutectic $0.725LiBH_4/0.275KBH_4$ are shown in Figure 1. The electrolyte composition was chosen to minimize the melting point (~110 °C, Figure S1) and to reduce the chance of any side reactions.[33] Samples were prepared by hand-grinding $LiBH_4$ and KBH_4, and then adding milled MgH_2/Sn with gentle mixing using a spatula. The mass fraction of hydride in the hydride + electrolyte system was ~50% (increasing the hydride fraction to practical levels, e.g., >~70%, was not the objective of this work and will be considered elsewhere). The dehydrogenation reactions were conducted under an initial H_2 pressure of 2 bar to prevent any significant direct dehydrogenation of MgH_2 forming Mg metal (the equilibrium temperature for MgH_2 at 2 bar H_2, T_{eq}(2 bar), is ~ 300 °C). Slow dehydrogenation was detected at 150 °C (Figure 1a). Without electrolyte, the rate was 0.0008 wt% H_2/h. With $LiBH_4$-KBH_4, the rate (with respect to the MgH_2 + Sn mass only) increased to 0.010 wt% H_2/h and with $LiBH_4$-KBH_4 additionally including $0.025MgI_2$, the rate was 0.020 wt% H_2/h. These rates are 12× and 25× higher, respectively, than the rate without electrolyte. At higher temperatures, smaller increases of 4.7× to 7.3× at 175 °C and 3.2× at 200 °C were observed. Figure 1b depicts the rates in Arrhenius form. Although there are too few temperatures for accurate estimates, the activation energy does appear to decrease significantly from ~150 kJ/mol-H_2 without electrolyte to ~100 kJ/mol-H_2 with the

0.725$LiBH_4$/0.275KBH_4 eutectic. We note that these activation energies are still much higher than the thermodynamic barrier of 39 kJ/mol-H_2, estimated from tabulated thermodynamic data for the pure phases. In addition to increased initial rates with the electrolytes, the dehydrogenation rates remained nearly constant until the reaction was almost complete. In contrast, without electrolyte the rate steadily decreases (i.e., at 200 °C, ~70 h, Figure 1), even though the extent of reaction was low. In preliminary similar work, nearly constant dehydrogenation rates were also seen in the MgH_2/Si system (Figure S2). In addition, preliminary measurements for MgH_2/Sn using several other potential electrolyte systems either appeared to decompose or showed similar or slower rates

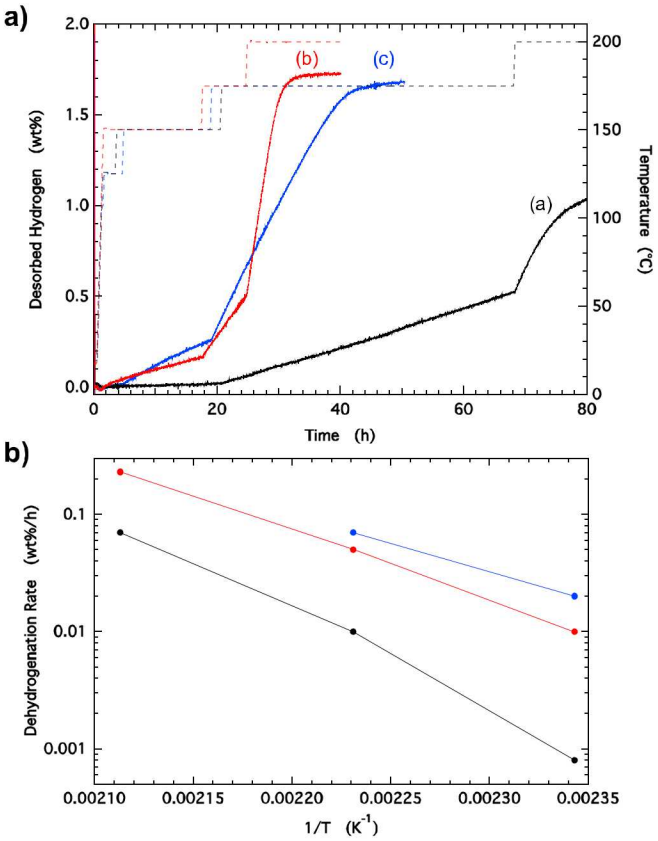

of dehydrogenation (see SI).

Figure 1. Dehydrogenation of MgH_2/Sn with and without electrolyte. Panel a) desorbed hydrogen (curve a, black) without electrolyte; (curve b, red) with added 0.725$LiBH_4$/0.275KBH_4, 50 wt% MgH_2/Sn; (curve c, blue) with added 0.725$LiBH_4$/0.275KBH_4 + 0.025MgI_2, 44 wt%

MgH_2/Sn; (dashed curves) corresponding temperatures, right axis. Panel b) dehydrogenation rates vs. inverse absolute temperate (determined from linear fits to the isothermal intervals; the uncertainties are ~5%, see SI). Desorbed hydrogen (wt%) and dehydrogenation rates (wt% H_2/h) are with respect to the MgH_2/Sn mass only. Dehydrogenation was conducted in an initial hydrogen pressure of 2 bar to suppress direct dehydrogenation of MgH_2 as well as any decomposition of the electrolyte.

To investigate reversibility, samples dehydrogenated with and without $LiBH_4$-KBH_4 electrolyte were treated in hydrogen at 920 bar to 1000 bar while decreasing the temperature from 215 °C to 175 °C, over 75 hours (Figure S3). Following this treatment, a second dehydrogenation was conducted. The results are shown in Figure 2. With the electrolyte, dehydrogenation of ~1.9 wt% occurred indicating nearly complete hydrogenation during the hydrogen treatment. This capacity is ~15% greater than the capacity for the initial dehydrogenation possibly indicating improved reaction as a result of cycling. Without electrolyte, at most only 0.3 wt% uptake occurred. We consider this capacity an upper limit because considerable hydrogen remained after the initial dehydrogenation, and this remaining hydrogen could have continued to evolve during the 2nd dehydrogenation.

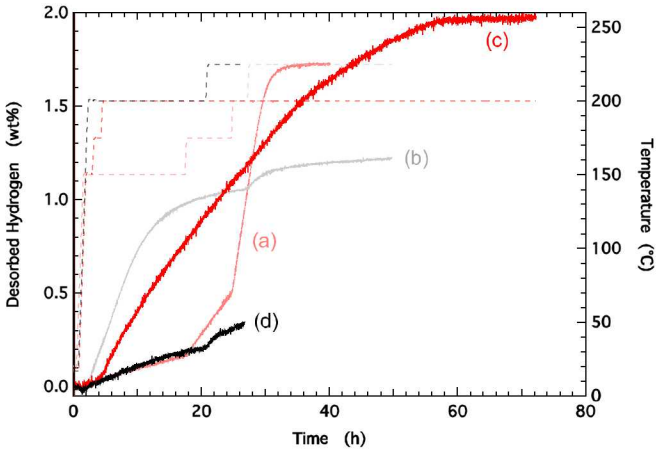

Figure 2. First and second cycle dehydrogenation of MgH_2/Sn with and without $LiBH_4$-KBH_4 eutectic electrolyte. 1st cycle dehydrogenation (a, light red) with electrolyte; (b, gray) without electrolyte. 2nd cycle dehydrogenation (c, dark red) with electrolyte; (d, black) without electrolyte. (dashed curves) Corresponding temperatures, right axis. Desorbed hydrogen (wt%) is with respect to the MgH_2/Sn mass only. Hydrogenation treatment between cycles was conducted at 920 bar to 1000 bar while decreasing the temperature from 215 °C to 175 °C, over 75 hr. Dehydrogenations were performed with an initial hydrogen pressure of 2 bar H_2. The dehydrogenation temperature was limited to 225 °C to avoid melting the Sn (T_m = 232 °C).

X-ray diffraction analysis confirmed the dehydrogenation measurements, as shown in Figures S4 and S5. Following dehydrogenation, Mg_2Sn was clearly seen both with and without electrolyte. After subsequent hydrogen treatment with the electrolyte, peaks for Mg_2Sn disappeared while those for MgH_2 and Sn grew, indicating significant rehydrogenation. In contrast, without electrolyte, similar patterns were seen before and after hydrogen treatment indicating that no or minimal reaction occurred.

Electrolyte-assisted hydrogenation of MgB_2. Samples of milled MgB_2 with and without electrolytes were treated in ~1000 bar hydrogen at 320 °C for 50 h (Figure S6). Two electrolytes were evaluated. The first was the $0.725LiBH_4/0.275KBH_4$ eutectic, the same electrolyte used with the MgH_2/Sn system described above. The second was a ternary alkali metal iodide with the composition 0.33LiI/0.33KI/0.33CsI, which melts at ~210 °C (Figure S7). To minimize any water content, this electrolyte was mixed and cycled to 300 °C several times prior to mixing with MgB_2. All three samples were treated in hydrogen simultaneously in a pressure vessel with multiple

individual sample holders. Treatment at 320 °C was chosen because previous work indicated only minor amounts of hydrogen uptake (<~1 wt%) occurred at this temperature.[34] Subsequent dehydrogenations of the hydrogen-treated samples are shown in Figure 3. Dehydrogenation of only ~0.3 wt% was observed for the MgB_2 without electrolyte, indicating minimal hydrogen uptake, as expected. In contrast, both samples with eutectic electrolytes showed significant dehydrogenation of ~6 wt% H_2 (with respect to the mass of MgB_2). Thus, including the electrolyte increased the hydrogen uptake by ~20×, to ~40% of completion. The initial rates at 250 °C to 300 °C for both eutectics were similar as seen by the similar slopes at ~9 h and 20 h, respectively. However, the rate with the 0.33LiI/0.33KI/0.33CsI eutectic decreased over time, ultimately requiring 350 °C to desorb ~6 wt% H_2, while with the $0.725LiBH_4/0.275KBH_4$ eutectic, 6 wt% H_2 was desorbed at 300 °C. Two additional samples with the 0.33LiI/0.33KI/0.33CsI eutectic, one with 31 wt% MgB_2 and another with 47 wt% MgB_2 (~1/2 the amount of eutectic), were similarly hydrogen treated but dehydrogenated using a different apparatus in a different laboratory. The results, shown in Figure S8, confirm those shown in Figure 3 and show that the improved hydrogen update persists for lower electrolyte fractions.

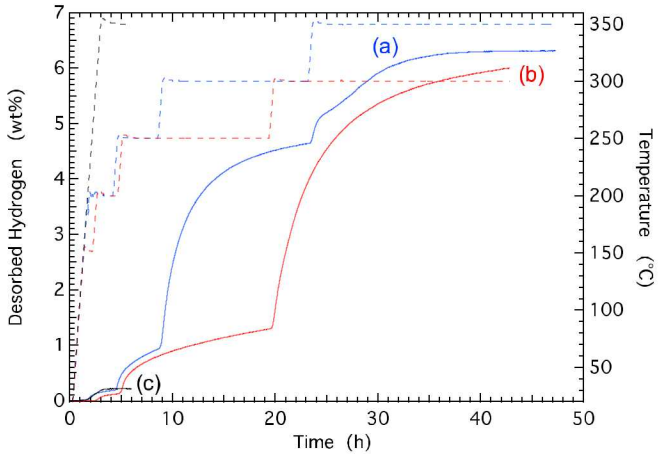

Figure 3. Dehydrogenation of MgB_2 following treatment in high pressure hydrogen with and without electrolytes. (a, blue) With 0.33LiI/0.33KI/0.33CsI eutectic, 31 wt% MgB_2; (b, red) with $0.725LiBH_4/0.275KBH_4$ eutectic, 46 wt% MgB_2; (c, black) without electrolyte; (dashed curves) corresponding temperatures, right axis. The inflection in the rate of (a) at 25 h may be associated with slight foaming which was detected when removing the sample. Desorbed hydrogen (wt%) is with respect to the MgB_2 mass only. Dehydrogenation with $0.725LiBH_4/0.275KBH_4$ eutectic was conducted into an initial pressure of 2 bar H_2; dehydrogenation with the 0.33LiI/0.33KI/0.33CsI eutectic was conducted into an initial vacuum.

The dehydrogenation results shown in Figure 3 are supported by ^{11}B NMR spectra before and after hydrogen treatment as shown in Figure 4. For the MgB_2 without the electrolyte, the ^{11}B NMR spectra before and after hydrogen treatment are nearly identical (Figure 4a). A small peak at -41 ppm indicates $[BH_4]^-$ species with a fraction of ~3% of the integrated ^{11}B signal area. In contrast, with the 0.33LiI/0.33KI/0.33CsI electrolyte after hydrogen treatment (Figure 4b) there is a large signal at -39 ppm with an area of 71%, while the area for MgB_2 decreases to 21%. There is also a small signal (4%) at -15 ppm corresponding to $[B_{12}H_{12}]^{2-}$ species. There are small shoulders on the -39 ppm peak that may indicate $[BH_4]^-$ species in different environments, possibly due to the presence of Li^+, K^+, and Cs^+ cations in the electrolyte.

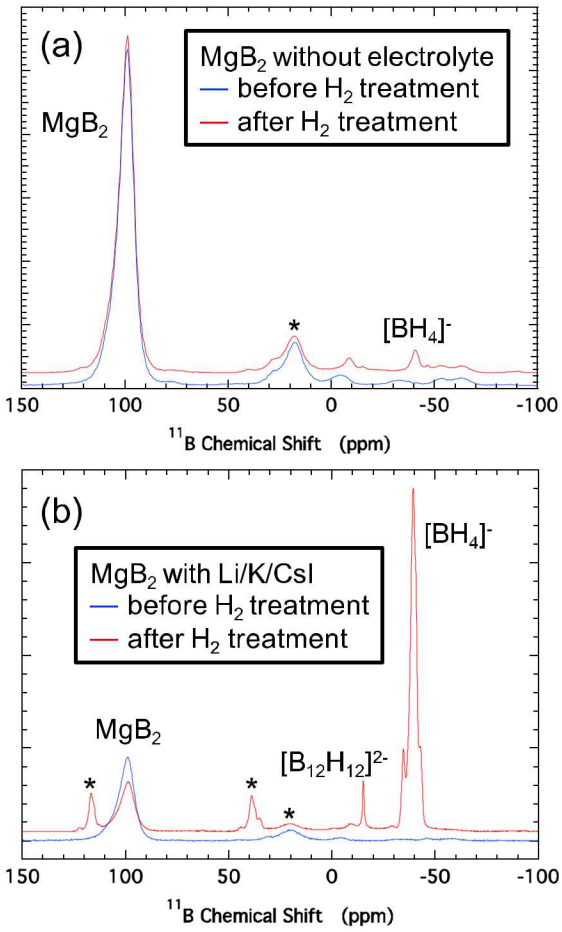

Figure 4. ^{11}B NMR spectra of MgB_2 with and without 0.33LiI/0.33KI/0.33CsI electrolyte before and after hydrogen treatment. (a) Without electrolyte, (blue) before hydrogen treatment, (red) after hydrogen treatment; (b) with 0.33LiI/0.33KI/0.33CsI electrolyte, (blue) before hydrogen treatment, (red) after hydrogen treatment. * indicates spinning sidebands.

Discussion

Although the mechanisms of these reactions have not yet been studied in detail, the presented results demonstrate the efficacy of using electrolytes with hydride materials and reveals the importance of inter-particle transport in hydrogen exchange. For the MgH_2/Sn system, the overall reaction is given by

$$2MgH_2 + Sn \rightarrow 2H_2 + Mg_2Sn \qquad (1)$$

Dehydrogenation must involve concerted reaction between MgH_2 and Sn because Mg metal, as a distinct phase, cannot form under the reaction conditions with the initial H_2 overpressure (ie, $P(H_2) \geq 2$ bar and $T_{reaction} \leq 225$ °C compared to $T_{eq}(2\ bar) \sim 300$ °C). Thus, Mg_2Sn can form only where MgH_2 and Sn are in direct contact at the atomic scale, as depicted in Figure 5.

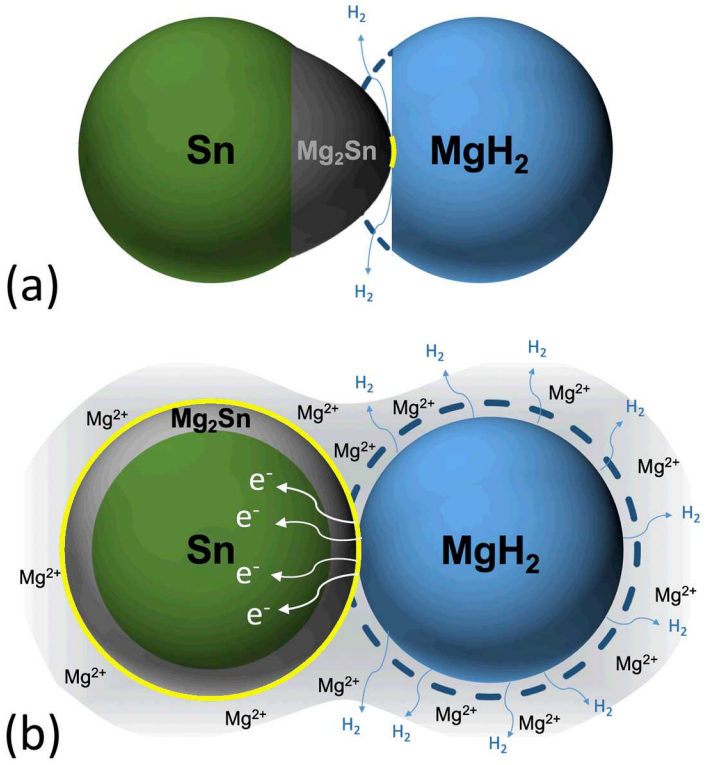

Figure 5. Dehydrogenation of MgH_2/Sn. (a) In the solid/solid reaction (without electrolyte) formation of Mg_2Sn only occurs where MgH_2 and Sn are in contact at the atomic level (shown in

yellow). (b) In an electrolyte, solubilized Mg^{2+} ions can diffuse through the electrolyte while electrons are conducted through solid-solid contacts enabling Mg_2Sn formation over the whole surface of a Sn particle (shown in yellow).

However, MgH_2 at the surface of a MgH_2 particle in contact with an electrolyte could dissociate releasing H_2 and forming a Mg^{2+} ion and two electrons. The Mg^{2+} ions could become solvated and diffuse in the electrolyte to the surface of a Sn particle while the electrons are transported through solid-solid contacts. At the Sn particle surface, $2Mg^{2+} + 4e^- + Sn$ can react to form Mg_2Sn. These steps are depicted in Figure 5 and given by

$$2MgH_2 \rightarrow 2Mg^{2+}(\text{sol-}MgH_2) + 4e^-(MgH_2) + 2H_2(g) \quad \text{dehydrogenation} \quad (2)$$

$$2Mg^{2+}(\text{sol-}MgH_2) \rightarrow 2Mg^{2+}(\text{sol-Sn}) \quad \text{diffusion in electrolyte} \quad (3)$$

$$4e^-(MgH_2) \rightarrow 4e^-(Sn) \quad \text{solid-solid conduction} \quad (4)$$

$$2Mg^{2+}(\text{sol-Sn}) + 4e^-(Sn) + Sn \rightarrow Mg_2Sn \quad \text{alloy formation} \quad (5)$$

where $2Mg^{2+}(\text{sol-}MgH_2)$ and $2Mg^{2+}(\text{sol-Sn})$ refer to Mg^{2+} ions solubilized at the surfaces of MgH_2 and Sn, and $4e^-(MgH_2)$ and $4e^-(Sn)$ refer to electrons in the MgH_2 and Sn solid phases, respectively. During diffusion (Eq. 3) the local environment of the $Mg^{2+}(sol)$ is presumably modified from that of the Li^+ and K^+ cations in the molten $LiBH_4/KBH_4$ eutectic to account for the 2+ charge. Given the nature of the eutectic, it is unlikely that MgH_2, a partially covalent hydride, or metallic Sn would be directly soluble. Although alloy formation (Eq. 5) may be initiated over the whole surface of the Sn that is wet by the electrolyte (Figure 5b), this step still involves solid state diffusion of Mg and/or Sn through the growing Mg_2Sn phase. Thus, this step may benefit from reduced particle sizes. The metallic nature of Sn may facilitate this reaction by enabling electron conduction (Eq. 4) from the MgH_2 (one reason that this system was chosen). Some support for

this scenario, is provided by the increased dehydrogenation rates observed when MgI_2 was added to the $LiBH_4$-KBH_4 eutectic (Figure 1). Without any added Mg salt, there would theoretically be no Mg^{2+} ions to initiate the reaction, although we suspect that, in this case, oxidization products (such as MgO or $Mg(OH)_2$) likely present at the MgH_2 particle surfaces[35] could provide some dissolved Mg^{2+} ions. With intentionally added MgI_2, the Mg^{2+} concentration may well be increased enabling faster reaction. Although the solubility of MgI_2 in the $LiBH_4$-KBH_4 eutectic is not known, iodide was chosen for its similar ionic size to $[BH_4]^-$, which should improve solubility.

For hydrogenation of MgB_2, hydrogen interacts, at least initially, with only a single phase. Based on equilibrium phases, hydrogenation could proceed through a mixed $MgB_{12}H_{12}/MgH_2$ step, although hydrogenation has been shown to proceed directly to $Mg(BH_4)_2$ during the initial hydrogenation step.[36] In this case, similarly enhanced transport of ionic species along the surface of MgB_2 particles could account for the increased hydrogen uptake. For example, the possibility of localized Mg^{2+} or $[BH_4]^-$ transport along the MgB_2/electrolyte interface could facilitate $Mg(BH_4)_2$ formation. In addition, some dissolution of $Mg(BH_4)_2$ as it forms may expose fresh MgB_2 surfaces for reaction. Even without atomic transport, the formation of $Mg(BH_4)_2$ from MgB_2 likely involves significant increase in surface area, at least in part associated with the large volume change of up to 400%. The free energy penalty associated with this increased area may be lowered by the presence of solid-liquid electrolyte as opposed to solid-gas interfacial energies.

These examples, MgH_2/Sn and MgB_2, have been discussed as limiting cases of enhanced inter-particle and particle surface transport. However, likely both inter-particle and surface transport

occur in both systems and can be facilitated by liquid electrolytes. In contrast, we expect that solid state diffusion within particles would likely not be affected.

In addition to atomic transport, inclusion of electrolytes may enhance the reactivity of solid phases by etching passivating surface layers. For example, specifically using the iodide-based 0.33LiI/0.33KI/0.33CsI eutectic (or halide-based electrolytes in general) may facilitate reaction by etching, or at least partially dissolving, surface oxides present on the MgB_2 surface.[36] This dissolution would expose MgB_2 to hydrogen analogous to the manner in which aqueous halide solutions are known to promote corrosion of metals, such as aluminum, that have passivating oxides.[37]

Ideally and most simply, an electrolyte would function only as a solvent for mobile ions or passivating surface layers without further participating or altering the overall hydrogen cycling reaction. However, to be suitable solvents for the hydride phase cations and be compatible with the hydrogen chemical potentials required for hydrogen cycling, possible electrolytes may likely need to be sufficiently chemically similar to the hydride phases that they do alter or participate in the desired overall reaction. For example, for MgH_2/Sn with the $LiBH_4$-KBH_4 electrolyte, Li_xSn alloys and $Mg(BH_4)_2$ are possible side reaction products. For the initial characterization performed in this work, significant side reaction was not observed. Specifically, the major phases observed by XRD after a single dehydrogenation and rehydrogenation cycle were Mg_2Sn and MgH_2 + Sn, respectively (Figure S4). Further work is needed to determine if side reaction products may accumulate slowly over multiple cycles. We note that although side reactions may ultimately occur, if meeting requirements, the overall hydride-electrolyte combination may be considered as a suitable hydrogen storage material system.

Conclusion

In summary, we have used electrolytes to improve the hydrogen cycling in multiple-phase hydrogen storage materials and shown significant improvements for the dehydrogenation and rehydrogenation of MgH_2/Sn and the hydrogenation of MgB_2. These results clearly indicate that inter-particle transport between different phases and/or transport over the surface of individual particles is an important aspect of the hydrogen cycling reaction that can be facilitated (and studied) using electrolytes. The compositions used in this study contained an excess of electrolyte (>50 wt% electrolyte mass fraction). To be useful for practical hydrogen storage applications, lower electrolyte fractions (e.g. <~25 wt%) would need to be demonstrated. We consider this a reasonable possibility given that optimized modern Li-ion batteries contain ~15 wt% electrolyte with respect to the full mass (active material + electrolyte mass). One path here is optimizing the particle sizes. Larger particles have lower surface area and therefore require less electrolyte to coat; however, they also have longer diffusion distances within and along particles. Moving forward, a wide range of electrolytes may be considered including other eutectics, solvents with dissolved salts, and ionic liquids, although thermal stability, chemical stability at hydride chemical potentials, and vapor pressure all present stringent requirements. Finally, it seems that the use of electrolytes could significantly improve the rates of hydrogen exchange in perhaps many other complex hydride materials including metal alanates, amides, borohydrides, and destabilized systems.

Supporting information

Experimental methods, other potential electrolytes investigated, Figures S1 to S8.

Notes

** Current address: Phillips 66 Research Center, Bartlesville, OK 74003.

The authors declare no competing financial interests.

Acknowledgments

This work was supported by the U. S. Department of Energy under contract DE-EE0007849. The NMR facility at the California Institute of Technology was supported by the National Science Foundation (NSF) under Grant Number 9724240 and partially supported by the MRSEC Program of the NSF under Award Number DMR-520565. Sandia authors gratefully acknowledge research support from the U.S. Department of Energy, Office of Energy Efficiency and Renewable Energy, Fuel Cell Technologies Office through the Hydrogen Storage Materials Advanced Research Consortium (HyMARC). Sandia National Laboratories is a multimission laboratory managed and operated by National Technology and Engineering Solutions of Sandia, LLC., a wholly owned subsidiary of Honeywell International, Inc., for the U.S. Department of Energy's National Nuclear Security Administration under contract DE-NA-0003525. This paper describes objective technical results and analysis. Any subjective views or opinions that might be expressed in the paper do not necessarily represent the views of the U.S. Department of Energy or the United States Government.

References

(1) Li, H.-W.; Wu, G.; Chen, P. Solid Hydrogen Storage Materials: Non-interstitial Hydrides, Chap 15 in *Hydrogen Energy Engineering* Sasaki, K.; Li, H.-W.; Hayashi, A.; Yamabe, J.; Ogura, T.; Lyth, S. M. Eds., **2016**, Springer Japan, DOI 10.1007/978-4-431-56042-5_15.

(2) Callini, E.; Atakli, Z. O. K.; Hauback, B. C.; Orimo, S.; Jensen, C.; Dornheim, M.; Grant, D.; Cho, Y. W.; Chen, P.; Hjörvarsson, B.; et al. Complex and Liquid Hydrides for Energy Storage. *Appl. Phys. A* **2016**, *122:353*, DOI 10.1007/s00339-016-9881-5.

(3) Stavila, V.; Klebanoff, L.; Vajo, J. J.; Chen. P. Development of On-Board Reversible Complex Metal Hydrides for Hydrogen Storage, Chap. 6 in *Hydrogen Storage Technology Materials and Applications* Klebanoff, L. ed., **2013**, CRC Press.

(4) Vajo, J. J.; Olson, G. L. Hydrogen Storage in Destabilized Chemical Systems. *Scr. Mater.* **2007**, *56*, 829– 834, DOI: 10.1016/j.scriptamat.2007.01.002.

(5) Dornheim, M.; Doppiu, S.; Barkhordarian, G.; Bösenberg, U.; Klassen, T.; Gutfleisch, O.;

Bormann, R. Hydrogen Storage in Magnesium-Based Hydrides and Hydride Composites. *Scr. Mater.* **2007**, 56, 841– 846, DOI: 10.1016/j.scriptamat.2007.01.003.

(6) Frankcombe, F.; Proposed Mechanisms for the Catalytic Activity of Ti in $NaAlH_4$. *Chem. Rev.* **2012**, *112*, 2164-2178, DOI: 10.1021/cr2001838.

(7) Yu, X.; Tang, Z.; Sun, D.; Ouyang, L.; Zhu, M. Recent Advances and Remaining Challenges of Nanostructured Materials for Hydrogen Storage Applications. *Prog. Mater. Sci.* **2017**, *88*, 1-48, DOI: 10.1016/j.pmatsci.2017.03.001.

(8) de Jongh, P. E.; Allendorf, M.; Vajo, J. J.; Zlotea, C. Nanoconfined Light Metal Hydrides for Reversible Hydrogen Storage. *MRS Bull.* **2013**, *38*, 488– 494.

(9) Vajo, J. J. Influence of Nano-Confinement on the Thermodynamics and Dehydrogenation Kinetics of Metal Hydrides. *Curr. Opin. Sol. State Mater, Sci.* **2011**, *15*, 52-61, DOI: 10.1016/j.cossms.2010.11.001.

(10) Zheng, X.; Xu, W.; Xiong, Z.; Chua, Y.; Wu, G.; Qin, S.; Chen, H.; Chen, P. Ambient Temperature Hydrogen Desorption from $LiAlH_4$-$LiNH_2$ Mediated by HMPA. *J. Mater. Chem.* **2009**, *19*, 8426-8431.

(11) Zheng, X.; Xiong, Z.; Qin, S.; Chua, Y.; Chen, H.; Chen, P. Dehydrogenation of $LiAlH_4$ in HMPA. *Int. J. Hy.* Energy **2008**, *33*, 3346-3350, DOI: 10.1016/j.ijhydene.2008.04.010.

(12) Xiong, Z.; Chua, Y.-S.; Wu, G,; Xu, W.; Chen, P.; Shaw, W.; Karamkar, A.; Linehan, J. Smurthwaite, T.; Autrey, T. Interaction of Lithium Hydride and Ammonia Borane in THF. *Chem. Comm.* **2008**, 5595-5597, DOI: 10.1039/b812576g.

(13) Zhang, S.; Taniguchi, A.; Xu, Q.; Takeichi, N. Takeshita, H. T.; Kuriyama, N.; Kiyobayashi, T.; Understanding the Effect of Titanium Species on the Decomposition of Alanates in Homogeneous Solution. *J. Alloy. Compds.* **2006,** *413*, 218-221, DOI: 10.1016/j.jallcom.2005.04.211.

(14) Mohtadi, R.; Sivasubramanian, P.; Hydrogen Release from Complex Metal Hydrides by Solvation in Ionic Liquids. **2014**, US patent 8,771,635.

(15) Humphries, T. D.; Birkmire, D.; McGrady, G. S.; Hauback, B.; Jensen, C. M.; Regeneration of $LiAlH_4$ at Sub-Ambient Temperatures Studied by Multinuclear NMR Spectroscopy. *J. Alloy. Compds.* **2017**, *723*, 1150-1154 DOI: 10.1016/j.jallcom.2017.06.300.

(16) Chong, M.; Matsuo, M.; Orimo, S.; Autrey, T.; Jensen, C. M.; Selective Reversible Hydrogenation of $Mg(B_3H_8)_2/MgH_2$ to $Mg(BH_4)_2$: Pathway to Reversible Borane-Based Hydrogen Storage? *Inorg. Chem.* **2015**, *54*, 4120-4125, DOI: 10.1021/acs.inorgchem.5b00373.

(17) Ni, C.; L. Yang, Muckerman, J. T.; Graetz, J.; Aluminum Hydride Separation using N – Alkylmorpholine. *J. Phys. Chem. C* **2013**, *117* 14983.

(18) Graetz, J.; Wegrzyn, J.; Reilly, J. J. Regeneration of Lithium Aluminum Hydride ($LiAlH_4$). *J. Amer. Chem. Soc*. **2008**, *130*, 17790.

(19) Wang. J.; Ebner. A. D.; Ritter, J. A.; Synthesis of Metal Complex Hydrides for hydrogen Storage. *J. Phys. Chem. C* **2007**, *111*, 14917-14924, DOI: 10.1021/jp072788e.

(20) Wang. J.; Ebner. A. D.; Ritter, J. A.; Physiochemical Pathway for Cyclic Dehydrogenation and Rehydrogenation of $LiAlH_4$. *J. Am. Chem. Soc.* **2006**, *128*, 5949-5954, DOI: 10.1021/ja060045l.

(21) Wang, H.; Wu, G.; Cao, H.; Pistidda, C.; Chaudhary A.-L.; Garroni, S.; Dornheim, M.; Chen, P. Near Ambient Condition Hydrogen Storage in a Synergized Tricomponent Hydride System. *Adv. Energy Mater.* **2017**, 1602456, DOI: 10.1002/aenm.201602456.

(22) Tan, Y.; Guo, Y.; Li, S. Sun, W.; Zhu, Y.; Li, Q.; Yu, X.; A liquid-Based Eutectic System: $LiBH_4 \bullet NH_3$-$n NH_3BH_3$ with High Dehydrogenation Capacity at Moderate Temperature. *J. Mater. Chem.* **2011**, *21*, 14509-14515, DOI: 10.1039/cljm11158b.

(23) Graham, K. R.; Kemmitt, T.; Bowden, M. E.; High Capacity Hydrogen Storage in a Hybrid Ammonia Borane-Lithium Amide Material. *Energy Environ. Sci.* **2009**, *2*, 706-710, DOI: 10.1039/b901082c.

(24) Crivello, J.-C.; Denys, R. V.; Dornheim, M.; Felderhoff, M.; Grant, D. M.; Huot, J.; Jensen, T. R.; de Jongh, P.; Latroche, M.; Walker, et al.; V. A. Mg-Based Compounds for Hydrogen and Energy Storage. *Appl. Phys. A* **2016**, *122:85*, DOI: 10.1007/s00339-016-9601-1.

(25) Chaudhary, A.-L.; Paskevicius, M.; Sheppard, D. A.; Buckley, C. E.; Thermodynamic Destabilization of MgH_2 and $NaMgH_3$ using Group IV Elements Si, Ge, or Sn. *J. Alloys Compd.* **2015**, *623*, 109-116.

(26) Janot, R.; Cuevas, F.; Latroch, M. Percheron-Guégan, A.; Influence of Crystallinity on the Structural and Hydrogenation Properties of Mg_2X Phases (X = Ni, Si, Ge, Sn). *Intermetallics* **2006**, *14*, 163-169, DOI: 10.1016/j.intermet.2005.05.003.

(27) Chaudhary, A.-L.; Sheppard, D. A.; Paskevicius, M; Webb, C. J.; Gray, E. M. Buckley, C. E. Mg_2Si Nanoparticle Synthesis for High Pressure Hydrogenation. *J. Phys Chem. C* **2014**, *118*, 1240-1247, DOI: 10.1021/jp40865g.

(28) Polanski, M.; Bystrzycki, J.; The Influence of Different Additives on the Solid-State Reaction of Magnesium Hydride (MgH_2) with Si. *Int. J. Hydrog. Energy* **2009**, *34*, 7692-7699, DOI: 10.1016/j.ijhydene.2009.06.002.

(29) Vajo, J. J.; Mertens, F.; Ahn, C. C.; Bowman Jr., R. C.; Fultz, B.; Altering Hydrogen Storage Properties by Hydride Destabilization through Alloy Formation: LiH and MgH_2 Destabilized with Si. *J. Phys. Chem. B* **2004**, *108,* 13977-13983.

(30) Zavorotynska, O.; El-Karbachi, A.; Deledda, S. Hauback, B. Recent Progress in Magnesium Borohydride $Mg(BH_4)_2$: Fundamentals and Applications for Energy Storage. *Int. J. Hydrog. Energy* **2016**, *41*, 14387-14403, DOI: 10.1016/j.ijhydene.2016.02.015.

(31) Allendorf, M. D.; Stavila, V.; White, J. L.; Wang, T. C.; He, Y.; Klebanoff, L. E.; Kolasinski, R. D.; El Gabaly, F. Zhao, X. HyMARC: Sandia's Technical Effort. *Hydrogen and Fuel Cells Program 2018 Annual Merit Review and Peer Evaluation.* **2018** https://www.hydrogen.energy.gov/pdfs/review18/st128_allendorf_2018_o.pdf.

(32) Severa, G.; Rönnebro, E.; Jensen, C. M. Direct Hydrogenation of Magnesium Boride to Magnesium Borohydride. *Chem Commun.* **2010**, *46*, 421-423.

(33) Ley, M. B.; Roedern, E.; Jensen, T. R.; Eutectic Melting of $LiBH_4$-KBH_4. *Phys. Chem. Chem. Phys.* **2014**, *16*, 24194-24199, DOI: 10.1039/c4cp03207a.

(34) Newhouse, R. J. Part I. Femtosecond Transient Absorption Studies of Metal and Semiconductor Nanostructures; Part 2. Synthesis and Characterization of Complex Hydride Materials for Hydrogen Storage Applications. Ph.D. Dissertation, University of California Santa Cruz, Santa Cruz, CA, 2011.

(35) House, S. D.; Vajo, J. J.; Ren, C.; Zaluzec, N. J.; Rockett, A. A.; Robertson, I. M.; Impact of Initial Catalyst Form on the 3D Structure and Performance of Ball-Milled Ni-Catalyzed MgH_2 for Hydrogen Storage. *Int. J. Hydrog. Energy* **2017**, *42*, 5177-5187, DOI: 10.1016/j.ijhydene.2017.01.205.

(36) Ray, K. G.; Klebanoff, L. E.; Lee, J. R. I.; Stavila, V.; Heo, T. W.; Shea, P.; Baker, A. A.; Kang, S.; Bagge-Hansen, M.; Liu, Y.-S.; et al.; Elucidating the Mechanism of MgB_2 Initial Hydrogenation *via* a Combined Experimental-Theoretical Study. *Phys. Chem. Chem. Phys.* **2017**, *19*, 22646. DOI: 10.1039/c7cp03709k.

(37) Natishan, P. M.; O'Grady, W. E. Chloride Ion Interactions with Oxide-Covered Aluminum Leading to Pitting Corrosion: A Review. *J. Electrochem. Soc.* **2014**, *161*, C421-C432.

TOC Graphic

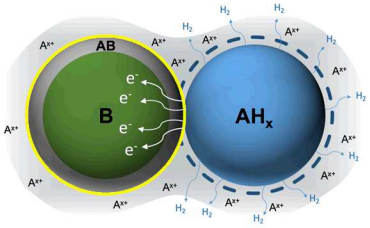

$$\underline{AH_x} \rightarrow A^{x+} + e^- + x/2H_2$$
$$A^{x+} + e^- + B \rightarrow AB$$